Received: 24 January 2022 | Revised: 16 June 2022 | Accepted: 17 June 2022 | Published on: 25 July 2022

DOI: 10.1002/mrm.29383

RESEARCH ARTICLE

Magnetic Resonance in Medicine

Reproducibility of rapid multi-parameter mapping at 3T and 7T with highly segmented and accelerated 3D-EPI

Difei Wang[1] | **Philipp Ehses**[1] | **Tony Stöcker**[1,2] | **Rüdiger Stirnberg**[1]

[1]German Center for Neurodegenerative Diseases (DZNE), Bonn, Germany

[2]Department of Physics and Astronomy, University of Bonn, Bonn, Germany

Correspondence
Tony Stöcker, German Center for Neurodegenerative Diseases (DZNE), Venusberg-Campus 1, Building 99, 53127 Bonn, Germany.
Email: tony.stoecker@dzne.de,

Funding information
EU(AROMA); EU Joint Programme—Neurodegenerative Disease Research (JPND); SCAIFIELD project; Bundesministerium für Bildung und Forschung, Grant/Award Number: 01ED2109A; German Federal Ministry of Education and Research; European Union Horizon 2020 Research and Innovation program, Grant/Award Number: 885876

Purpose: Quantitative multi-parameter mapping (MPM) has been shown to provide good longitudinal and cross-sectional reproducibility for clinical research. Unfortunately, acquisition times (TAs) are typically infeasible for routine scanning at high resolutions.

Methods: A fast whole-brain MPM protocol based on interleaved multi-shot 3D-EPI with controlled aliasing (SC-EPI) at 3T and 7T is proposed and compared with MPM using a standard spoiled gradient echo (FLASH) sequence. Four parameters (R_1, PD, R_2^*, and MTsat) were measured in less than 3 min at 1 mm isotropic resolution. Five subjects went through the same scanning sessions twice at each scanner. The intra-subject coefficient of variation (scan–rescan) (CoV) was estimated for each protocol and scanner to assess the longitudinal reproducibility.

Results: At 3T, the CoV of SC-EPI ranged between 1.2%–4.8% for PD and R_1, 2.8%–10.6% for R_2^* and MTsat, which was comparable with FLASH (0.6%–4.9% for PD and R_1, 2.6%–11.3% for R_2^* and MTsat). At 7T, where the SC-EPI TA was reduced to ∼2 min, the CoV of SC-EPI (1.4%–10.6% for PD, R_1, and R_2^*) was 1.2–2.4 times larger than the CoV of FLASH (1.0%–15%) and MTsat showed much higher variability across subjects. The SC-EPI-MPM protocol at 3T showed high reproducibility and yielded stable quantitative maps at a clinically feasible resolution and scan time, whereas at 7T, MT saturation homogeneity needs to be improved.

Conclusion: SC-EPI-based MPM is feasible as an additional MRI modality in clinical or population studies where the parameters offer great potential as biomarkers.

KEYWORDS
EPI, MPM, MT, PD, T_1, T_2^*

1 | INTRODUCTION

Neurodegeneration has been investigated using conventional MRI in different studies.[1–3] Pathologies related to distinct lesion patterns can be found on conventional MRI. But plain MR images with a certain contrast alone are not sensitive enough to detect the progress of anatomical and functional changes, especially in the incipient

stages. Advanced MRI techniques with feasible scan time provide additional biomarkers for diagnosis at an early disease stage with standardized scanning protocols, post-processing methods, and evaluation methods.[4]

In recent years, quantitative MRI is drawing more attention in the clinical field. Many applications and studies require quantitative estimates of physical properties in physical units. Examples for common quantitative measurements with physiological applications as biomarkers are T_1 and T_2^* relaxation times to measure tissue oxygenation,[5] apparent diffusion coefficient to detect ischemic stroke,[6] tissue iron fraction for diagnosis of iron overload.[7]

Conventional MRI protocols include T_1-weighted sequences for anatomical structural evaluation, T_2-weighted sequences, which are particularly sensitive to tissue property changes[8] and proton density-weighted sequences. Multi-parameter mapping (MPM), which combines T_1-, PD-, MT-weighted images, is meant to provide quantitative $R_1 = 1/T_1$ (longitudinal relaxation rate), PD (proton density), MTsat (magnetization transfer saturation) and $R_2^* = 1/T_2^*$ (effective transverse relaxation rate) parameter maps.[9] It has been proven to show high reproducibility and repeatability across different sites, scanners and time points.[10]

A typical MPM protocol is composed of three multi-echo spoiled gradient echo scans acquired in approximately 15–20 min at 3T. These will be referred to FLASH scans in this work. Although the total acquisition time (TA) of MPM alone is clinically feasible, adding MPM to a conventional MRI protocol may not be feasible. One way to reduce MPM scan time is to reduce spatial resolution.[11] Alternatively, advanced parallel imaging techniques can be explored. We propose a fast MPM protocol that combines state-of-the-art 2D-CAIPIRINHA parallel imaging[12] with interleaved multi-shot three-dimensional (3D) EPI. In essence, such a segmented k-space blipped-CAIPI (skipped-CAIPI) 3D-EPI sequence[13] corresponds to a FLASH sequence with an EPI factor freely adjustable via the segmentation factor. An EPI factor >1 means that more than one k-space line is acquired per shot to speed up MR imaging. When using a relatively small EPI factor, the acquired lines per shot are significantly spaced apart. K-space data acquisition is completed in successive, interleaved shots with echo time shifting.[14] This results in a high effective phase encode bandwidth and minimal geometric distortions along the phase encoding direction as opposed to conventional EPI without segmentation. Interleaved multi-shot 3D-EPI with and without CAIPIRINHA sampling has already been used to reduce scan time for high-resolution, anatomical T_2^*-weighted imaging,[15,16] T_1-weighted imaging,[13,17] and quantitative susceptibility and T_2^* mapping.[18] To the best of our knowledge, it has not yet been used for rapid MPM.

Application of ultra-high field MRI provides increased signal sensitivity and higher SNR. The 7T studies provide high-resolution images within shorter TA and good temporal resolution. Ultra-high field MRI offers improved capability to detect abnormalities in cortical and subcortical structures.[19] A first generation 7T MRI scanner has been approved and distributed for clinical use. Therefore, we have decided to include MPM at 7T in this work focusing on clinical feasibility.

We propose fast MPM protocols using a multi-echo implementation of skipped-CAIPI 3D-EPI (SC-EPI)[18] at 3T and 7T. All weighted multi-echo images are acquired in less than 3 min. The parameter values and the scan–rescan reproducibility of each parameter were compared between FLASH-MPM and SC-EPI-MPM at 1 mm isotropic resolution. Inter- and intra-subject variability were studied in different regions of interest (ROIs) in Montreal Neurological Institute (MNI) space.

2 | METHODS

2.1 | Data acquisitions

Five healthy subjects were scanned on a Skyra 3T and a MAGNETOM 7T Plus scanners (Siemens Healthineers, Erlangen, Germany) after giving informed consent according to the local institutional review board regulations. A 32-channel head receive coil was used at each scanner. For RF transmission, the body coil was used at 3T. At 7T, a single-channel coil surrounding the receive coil was used for circular polarized RF transmission. Scan–rescan studies were performed in the way that each subject exited and re-entered the scanner after a break of at least 10 min outside the scanner room. At 7T, two dielectric bags were placed between coil and head, close to the ears, which helps to reduce the transmit field inhomogeneity.[20] To minimize Rician noise levels in low-signal areas of the image magnitudes (e.g., ventricles in T_1w images), a vendor-provided, complex-valued coil combination based on a single-channel phase reference measurement[21] was applied instead of the default sum-of-square coil combination mode in both SC-EPI and FLASH sequences.

A series of MPM experiments were performed at 3T and 7T using SC-EPI and FLASH for comparison. In all sequences, a single rectangular small-bandwidth excitation pulse (2.4 ms at 3T; 1.0 ms at 7T) was used to simultaneously avoid chemical shift artifacts[22] and minimize MT bias.[23] Slice orientation was sagittal with frequency encoding along the head-feet direction.

FLASH readout: T_1w, PDw, and MTw contrasts were acquired using the vendor-provided multi-echo spoiled gradient echo sequence that underwent only a few

modifications: (i) a CAIPIRINHA undersampling option was implemented and the related, vendor-provided image reconstruction was used ("IcePAT"), even if no CAIPI shift was selected; (ii) spoiler gradients were slightly increased to correspond to 4π, 2π and zero voxel dephasing on frequency, primary and secondary (slice) phase encode axis in accordance with the EPI implementation; (iii) a rectangular small-bandwidth excitation pulse could be used (see above); (iv) MT saturation parameters were made adjustable.

3T: Gold standard protocols were set up according to the recommendations by Callaghan et al. (vendor sequence)[24] following the setup tutorial.[25] For the MTw scan, a Gaussian-shaped RF pulse (2 kHz off-resonant, 500°) and gradient spoilers were applied prior to each excitation. Other parameters were: 1 mm isotropic nominal resolution (91% primary and secondary phase encode resolution in accordance with[24] throughout all MPM scans in this work), $2 \times 1_{z0}$ parallel imaging undersampling, 6/8 partial Fourier imaging along the secondary phase encode direction z, w.l.o.g. Instead of the six originally proposed TEs, we used five equidistant TEs between 3.68 ms up to 13.53 ms to accommodate the prolonged small-bandwidth excitation. However, the original TRs were maintained at 18 ms/18 ms/37 ms (PDw/T_1w/MTw). The total acquisition time was TA = 15:32.

7T: The 3T protocol was modified in order to reduce scan time as much as feasible given the expected gain in SNR. With six equidistant TEs from 2.04 ms up to 12.23 ms, the TRs were reduced to 16 ms/16 ms/32 ms (PDw/T_1w/MTw). A $3 \times 2_{z1}$ CAIPIRINHA undersampling pattern was selected. At 7T, specific absorption rate (SAR) limits as well as the B_1^+ inhomogeneities pose challenges for the MT saturation. For each subject, a suitable whole-brain reference voltage and the maximum allowed MT flip angle (FA) to yield ~100% SAR was set up individually to reach a compromise between B_1^+ homogeneity and SAR limitation. The reference voltage and MT FA for the five subjects were: 244 V/250°, 260 V/240°, 260 V/240°, 270 V/230°, 270 V/230°. The total acquisition time was TA = 4:35.

SC-EPI readout: With our custom implementation, the multi-echo T_1w, PDw, and MTw images can be acquired in one acquisition (multi-contrast), i.e., three contrasts share a single initial FLASH autocalibration scan for parallel imaging reconstruction.[26] In order to reduce EPI factors to begin with, 6/8 partial Fourier imaging was performed along the primary instead of the secondary phase encode direction. A multi-echo EPI readout typically results in a wider TE spread and a longer TR than FLASH without introducing void times such that scanning efficiency is comparably high.[27] A pictorial comparison of the multi-contrast multi-echo SC-EPI sequence to the corresponding FLASH sequence is shown in Figure 1.

3T: A $16{\cdot}2 \times 2_{z1}$ skipped-CAIPI sampling without z-blips[13] was used (four-fold parallel imaging undersampling). The segmentation factor of 16 resulted in an EPI factor of 5. This corresponds to an eight-fold segmented $4 \times 1_{y2}$ shot-selective CAIPI sampling[28] and is comparable to recent works on rapid T_1-weighted 3D-EPI at 3T.[17] MT saturation was identical to the 3T FLASH MTw. Four gradient echo images were acquired at equidistant TEs between 5.4 and 29.1 ms resulting in TRs of 39 ms/39 ms/54 ms (PDw/T_1w/MTw). Despite the prolonged TRs, the FAs were not increased compared to the FLASH protocol.

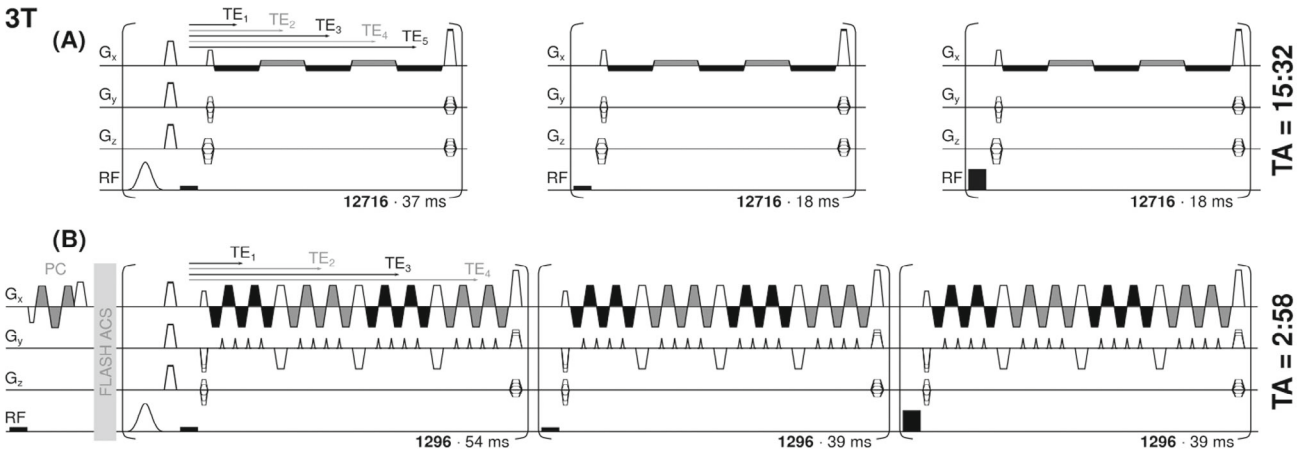

FIGURE 1 Schematic sequence diagrams of FLASH (A) and SC-EPI (B) at 3T, in the order MTw, PDw, T_1w. All three contrasts of SC-EPI share a single initial FLASH autocalibration scan for parallel imaging reconstruction[26] and a single initial phase correction scan.[13] Bold-face numbers at the bottom right of the shot-loops indicate the number of TRs per contrast. Non-bold numbers indicate the TR of each contrast. For visual clarity, the time axes between sequences are not true to scale

A single multi-contrast SC-EPI scan with one MTw, PDw, T_1w (in that order) took TA = 2:58.

7T: In accordance with the accelerated 7T FLASH protocol, a $13{\cdot}3 \times 2_{z1}$ skipped-CAIPI sampling was selected, resulting in an EPI factor of 4. Together with an increased gradient strength at 7T, this allowed for four shorter equidistant TEs between 3.7 and 23.7 ms and TRs of 36 ms/36 ms/50 ms (PDw/T_1w/MTw). Again, the MT FA was maximized individually to yield ∼100% SAR. Given that the TRs of the SC-EPI protocols were longer than the FLASH TRs, with identical reference voltages the MT FA for the five subjects could be increased compared to the FLASH MTw: 330°, 310°, 310°, 300°, 300°. A single multi-contrast SC-EPI scan with one MTw, PDw, T_1w (in that order) took TA = 2:15.

One subject was measured five times with the same multi-contrast-SC-EPI sequence at 3T and two times at 7T to approximately match the TA of the corresponding FLASH protocols (TA = 14:50 vs. 15:32 at 3T and TA = 4:30 vs. 4:35 at 7T). Accordingly, a time-matched MPM analysis was performed on the average of the five and two SC-EPI measurements, respectively. A summary of the most important MPM sequence parameters is given in Table 1.

Finally, for anatomical reference, a rapid T_1w MPRAGE sequence was acquired at 1 mm isotropic resolution using CAIPIRINHA and elliptical sampling.[29] At 7T, a high readout bandwidth multi-echo sequence version was used, and the four echoes were combined to an RMS image.[30]

2.2 | Transmit correction due to B_1^+ inhomogeneities

Before the MPM scans, a three-dimensional DREAM sequence (3DREAM)[31] was performed for simultaneous B_1^+ and B_0 mapping using $2 \times 2_{z1}$ CAIPIRINHA undersampling. At 3T, sequence parameters were as

TABLE 1 Multi-parameter mapping sequence parameters at 3T and 7T

	3T		7T	
PDw/T_1w/MTw	**FLASH**	**SC-EPI**	**FLASH**	**SC-EPI**
TR [ms]	18/18/37	39/39/54	16/16/32	36/36/50
FA [°]	4/25/6	4/25/6	4/25/6	4/25/6
TE [ms]	3.68, 6.15, 8.61, 11.07, 13.53	5.4, 13.3, 21.2, 29.1	2.04, 4.08, 6.12, 8.16, 10.20, 12.23	3.7, 8.7, 13.7, 18.7, 23.7
MT pulse FA [°]	500	500	250, 240, 240, 230, 230[a]	330, 310, 310, 300, 300[a]
MT off res. freq. [kHz]	2.0	2.0	2.0	2.0
Readout bandwidth [Hz/pixel]	480	1014	590	1314
Readout amplitude [mT/m]	11.3	23.8	13.8	30.9
Echo spacing [ms]	–	1.28	–	1.07
Eff. echo spacing [μs]	–	40	–	27
Phase encode bandwidth [Hz/pixel]	–	123.4	–	178.5
Matrix size	256 × 224 × 176	224 × 224 × 176	224 × 224 × 176	224 × 224 × 176
Elliptical scanning	On	Off	Off	Off
Partial Fourier	1 × 6/8	6/8 × 1	6/8 × 1	6/8 × 1
Parallel imaging	2 × 1	2 × 2	3 × 2	3 × 2
Slice CAIPI shift	–	1	1	1
Segmentation factor	–	16	–	13
EPI factor	–	5	–	4
Autocalibration scan	24 (integrated)	36 × 36	36 × 36	36 × 36
Shots	12 716	1296	4080	1053
Total TA [min:s][b]	15:32	2:58	4:35	2:15

[a] Subject-specific, maximum feasible MT pulse FA resulting in 100% SAR prediction.
[b] Total TAs include the autocalibration scan but not the 3DREAM prescan.

follows: sagittal orientation, 4 mm isotropic resolution, FOV = 160 × 200 × 200, nominal stimulated echo (STE) preparation FA $\alpha = 60^{\circ}$, FID and STE imaging FA $\beta = 8^{\circ}$, readout bandwidth of 1000 Hz/pixel, effective $TE_{STE} = 3.26$ ms, $TE_{FID} = 2.26$ ms, TA = 5 s. At 7T, the sequence parameters were: 5 mm isotropic resolution, FOV = 220 × 220 × 200, $\alpha = 50^{\circ}$ and $\beta = 7^{\circ}$, readout bandwidth of 1580 Hz/pixel, effective $TE_{STE} = 2.09$ ms, $TE_{FID} = 1.59$ ms, TA = 6 s. The actual 3DREAM FA is obtained as $\alpha_{3DREAM} = \arctan\sqrt{2\,|S^{STE}| \,/\, |S^{FID}|}$.[32] Here, S^{FID} and S^{STE} denote the global filter-matched[30] FID and virtual STE*[33] image magnitudes of the 3DREAM readout, which are usually TE-matched. By slightly increasing the STE preparation time, the off-resonance can be obtained from the image phase and the corresponding TE difference as $\Delta\omega = \left(\angle S^{FID} - \angle S^{STE}\right) / (TE_{FID} - TE_{STE})$.The typical transmit correction factor for MPM is given by the ratio of the 3DREAM FA and the nominal STE preparation FA:

$$f_T^{B_1}(x) = \alpha_{3DREAM}(x)/\alpha. \quad (1)$$

2.3 | Transmit correction due to B_0 inhomogeneities

Regions close to the sphenoid sinus and ethmoid sinus consist of different tissues, air, and bone. The local magnetic susceptibility differences lead to strong inhomogeneities of the magnetic field and thus to off-resonant spin frequencies, $\Delta\omega$, compared to the nominal Larmor frequency. A narrow-banded RF excitation pulse, as used in this work to suppress fat signal and to reduce unintended MT saturation, causes a reduced effective FA in these regions.[23] The reduced off-resonance FA can be calculated according to Freed et al.[34] For a rectangular pulse of duration τ, and a nominal FA α_{nom}, the effective FA is given analytically:

$$\alpha_{eff}(x) = \arccos\left(\cos\left(\Omega_{eff}(x)\cdot\tau\right) + \left(\frac{\Delta\omega}{\Omega_{eff}(x)}\right)^2 \cdot\left(1-\cos\left(\Omega_{eff}(x)\cdot\tau\right)\right)\right). \quad (2)$$

Here,

$$\Omega_{eff}(x) = \sqrt{(\Delta\omega)^2 + \left(\frac{\alpha_{nom}}{\tau}\cdot f_T^{B_1}(x)\right)^2} \quad (3)$$

denotes the off-resonant spin nutation frequency around the tilted, effective transmit field vector during the pulse. Note that the transmit correction factor, $f_T^{B_1}$, scales the nominal, on-resonant spin nutation frequency, α_{nom}/τ, around the nominal, transversal transmit field vector.

Consequently, for MPM using a narrow-banded rectangular excitation pulse, we have to use a different transmit correction factor:

$$f_T(x) = \alpha_{eff}(x)/\alpha_{nom}. \quad (4)$$

Note that in the on-resonant case ($\Delta\omega \to 0$), Equation (2) becomes $\alpha_{eff}(x) \to \alpha_{nom}\cdot f_T^{B_1}(x)$, and Equation (4) converges to the typical transmit correction factor for MPM according to Equation (1). However, in the off-resonant case ($\Delta\omega \neq 0$), f_T depends on the nominal MPM FA taken as a reference (e.g., 4°, 25° or 6°). For typical off-resonances in the brain at 3T and 7T, the corresponding f_T maps differ by <0.02% from each other. This is small compared to up to 5% difference between f_T and $f_T^{B_1}$. Since the established MPM transmit correction assumes only a single correction map, we calculated f_T based on an intermediate nominal FA of $\alpha_{nom} = 10^{\circ}$.

2.4 | RF receive field correction

A spatially dependent receive field sensitivity correction factor is required for PD calculation[35]: $A_{app} = A\cdot f_T = PD\cdot f_R\cdot f_T$.

A_{app} denotes the amplitude estimates obtained with the nominal FA. f_R is the receive correction factor.

At 3T, the receive field sensitivity map was acquired from the pair of head coil and body coil images ("HC-BC method") following the 3T recommendations[24,25] and similar to a recent multicenter study at 3T.[10] Note that this implies the assumption that the receive field sensitivity of the body coil is flat over the FOV, which does not strictly apply.[36] The imaging parameters were: 4 mm isotropic resolution, FOV = 176 × 224 × 256.

At 7T, the receive field sensitivity of the body coil is even more inhomogeneous. Thus, receive field correction was applied using Unified Segmentation.[37] This approach can be considered at 3T as well.[36] A detailed discussion of receive field correction methods can be found in the hMRI toolbox tutorial paper.[38]

2.5 | Estimation and analysis of parameter maps

R_1, PD, MTsat, and R_2^* maps were estimated from the multi-echo data using the hMRI toolbox v0.2.2[38] implemented in SPM12 (https://www.fil.ion.ucl.ac.uk/spm/software/spm12/). The hMRI toolbox uses all signals extrapolated to TE = 0 for parameter estimation.[9,38] R_1 maps were corrected for residual bias caused by imperfect spoiling.[39,40] R_2^* was estimated from all echoes

and contrasts simultaneously by ordinary least square fit.[41] The hMRI toolbox calibrates WM PD values to 69%.[38,42] PD values of other tissues are scaled accordingly. For receive and transmit field correction, the maps f_R and f_T were passed to the toolbox. All quantitative maps were normalized into MNI space using DARTEL tools[43] in SPM12.

For each parameter, subject-wise coefficient of variation (CoV) maps of all parameters were calculated separately for SC-EPI and FLASH. From these, the RMS CoV was calculated in various ROIs per subject. RMS-CoV values that exceed the first and third quartile by more than 1.5 times the interquartile range are considered outliers. The ROIs of caudate, hippocampus, pallidum, putamen, thalamus, and cerebral white matter (WM) were taken from the Harvard-Oxford Atlas with a threshold of 99%. The body of corpus callosum and middle cerebellar peduncle were taken from the Juelich ICBM-DTI-81 White-Matter atlas eroded three times for a unified mask across subjects. The whole-brain gray matter (GM) and WM masks were the averaged masks for GM and WM (tissue probability maps with a threshold of 60%) from scan–rescan MTw images per subject per scanners (3T and 7T).

3 | RESULTS

3.1 | Image quality of SC-EPI

Example axial, sagittal, and coronal slices of the first TE of MTw-, PDw-, T_1w-images acquired with SC-EPI and FLASH for a single representative subject are shown in Figure 2 at 3T and 7T. The amount of distortion in the SC-EPI images is visualized by overlaid contour lines of the WM/GM boundary taken from the tissue probability maps of M(EM)PRAGE generated from the hMRI toolbox.[38] Figure 3 shows corresponding axial and sagittal MTw slices more severely affected by susceptibility-related artifacts.

By visual inspection, no differences are observed between SC-EPI and FLASH in terms of geometric distortions and signal dropouts. The latter are due to the

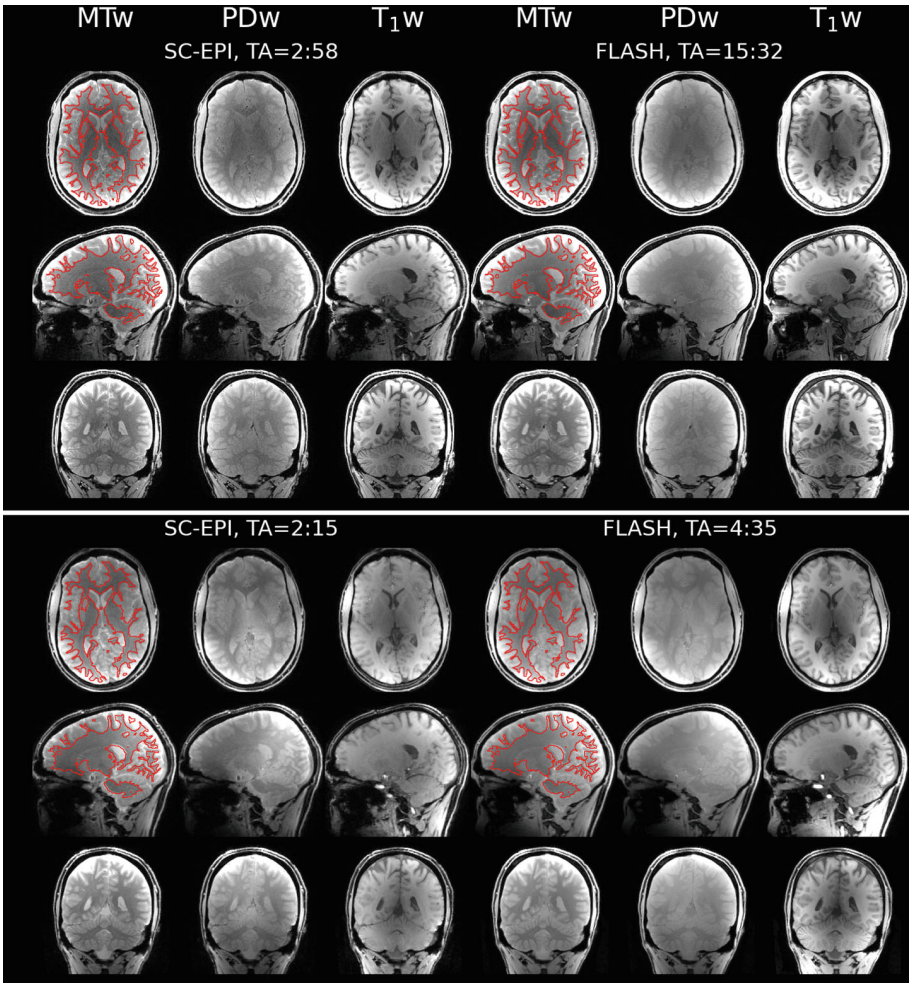

FIGURE 2 Axial, sagittal, and coronal slices of MT-, PD-, T_1-weighted images using the SC-EPI and FLASH sequence for a single, representative volunteer at 3T (top panel) and 7T (bottom panel). The contour lines of WM masks (red), taken from the segmentation of M(EM)PRAGE images at 3T and 7T, respectively, were overlaid on MTw images. The total TA of each sequence is also listed

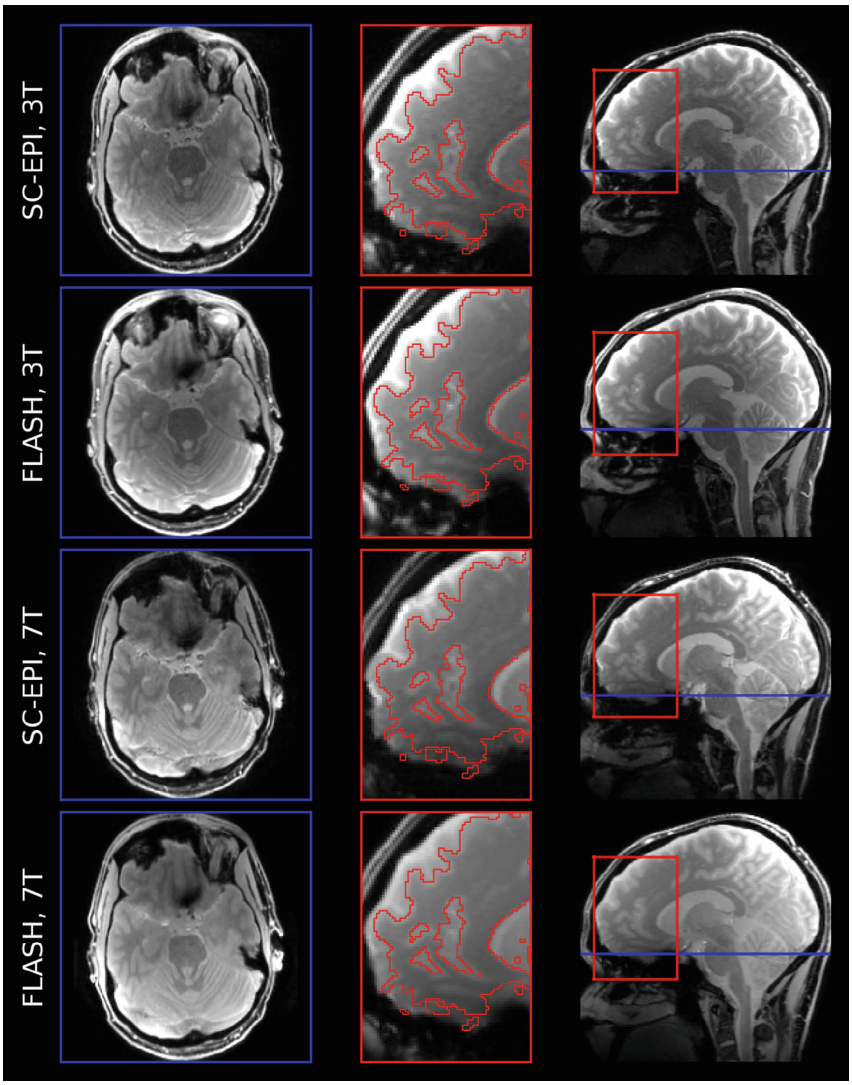

FIGURE 3 Axial and sagittal slices of the first TE (from top to bottom: 5.4, 3.68, 3.7, 2.04 ms) of MTw images showing the regions most severely affected by susceptibility-induced artifacts. MPRAGE-based contour lines of WM are overlaid on the zoomed sagittal view of the frontal lobe. Minimal geometric distortions occur along the anteroposterior phase encode direction for SC-EPI and along the head-feet readout direction for FLASH, respectively. Signal dropouts above the sinus are comparable despite the different readout, TEs, and field strengths

narrow-banded water excitation pulse (Supporting Information Figure S1, which is available online). The contrast for each weighting differs between SC-EPI and FLASH due to the different TRs used and TEs displayed. The soft tissue contrast (MT-weighted) is sufficient for tissue segmentation using SC-EPI, despite a reduced SNR due to the short TA compared to FLASH.

3.2 | Quantitative parameter maps

Quantitative high-quality R_1, PD, MTsat, and R_2^* maps generated from the SC-EPI and FLASH images are shown in Figure 4 for a single subject in original space. The maps labeled as 'EPI-TM' result from SC-EPI data acquired and averaged five times at 3T and twice at 7T for approximate time-matching with FLASH. All maps show good WM/GM contrast and different anatomical structures, for example caudate nucleus, putamen, thalamus, as well as GM structures in the cerebral cortex. In contrast to the weighted images, the parameter maps show better whole-brain homogeneity, also at 7T. Only the MTsat maps at 7T show lower values and worse soft tissue contrast, especially in the temporal lobe and cerebellum, regardless of the sequence used. Supporting Information Figure S2 shows the same 3T and 7T maps in a central sagittal slice.

3.3 | Multi-subject parameter comparison

Absolute differences of the parameters between the SC-EPI and FLASH protocols were assessed by comparing the mean parameter values in the whole-brain WM and GM ROIs, as plotted in Figure 5 and listed in Table 2. R_1 estimates of SC-EPI were 2.7%–5.8% higher than R_1 estimates of FLASH at 3T, and 10.7%–11.1% higher at 7T, the same applies to MTsat values. PD values were around 69% for WM (the MPM calibration value for WM[42]), while PD of SC-EPI was higher than of FLASH in GM. In GM, R_2^*

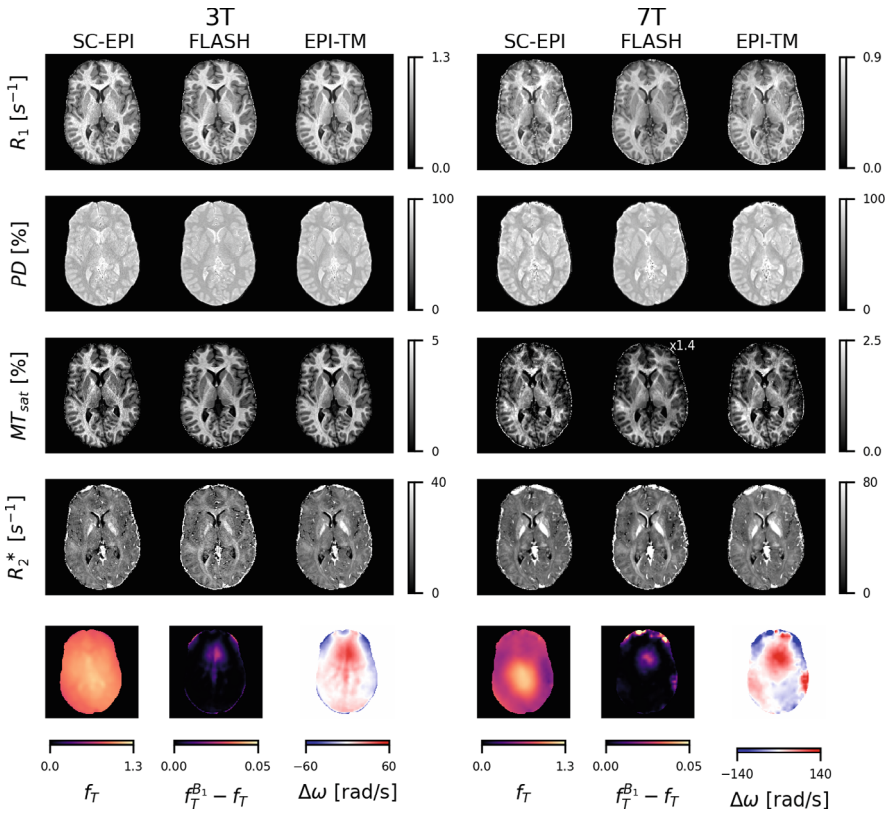

FIGURE 4 Parameter maps of SC-EPI and FLASH for a single subject scanned at 3T and 7T, including repeated SC-EPI for time-matching with the FLASH (EPI-TM). The MTsat map of FLASH at 7T was multiplied by a factor of 1.4 for a better comparison to the MTsat map of SC-EPI, which was acquired with a higher MT pulse FA. The f_T (transmit field correction) maps are shown along with difference to the conventional correction map without B_0 correction, as well as the corresponding off-resonance map, $\Delta\omega$

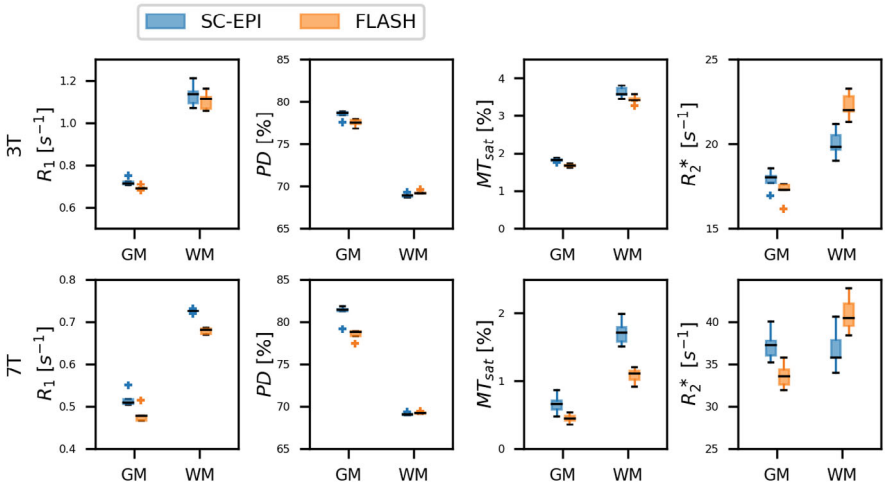

FIGURE 5 Mean values of parameter maps across scans and subjects for R_1, PD, MTsat, and R_2^* (box plot). ROIs: whole-brain GM and whole-brain WM. The outliers are marked as '+' in the corresponding color. MTsat values at 7T are expected to vary across subjects and sequences due to different MTsat FAs applied

values of SC-EPI were ~3.6% higher than those of FLASH at 3T, and 9.7% higher at 7T. In WM, R_2^* values of SC-EPI were ~9.8% smaller than R_2^* values of FLASH at both field strengths. Phantom R_1 and R_2^* data at 3T are shown in Supporting Information Figure S3.

3.4 | Multi-subject reproducibility analysis

Figure 6 shows the CoV maps for all parameters for the representative subject at 3T and 7T. The SC-EPI and FLASH box plots in Figure 7 include CoVs in each ROI of five subjects using SC-EPI, FLASH and time-matched EPI-TM acquisition protocols. Generally, the inter-scan SC-EPI RMS-CoV are in the same order of magnitude as the FLASH, excluding some outliers.

At 3T, the RMS-CoV for WM and GM was about 1%–3% for SC-EPI-PD (Figure 7, blue) and FLASH-PD (Figure 7, orange); about 2%–6% for SC-EPI-R_1 and 1%–4% for FLASH-R_1, as well as 5%–8% for SC-EPI-MTsat and 2%–5% for FLASH-MTsat. The RMS-CoVs for R_2^* were very similar and below 12% for both sequences excluding outliers. The highest CoVs were found for the R_2^*

TABLE 2 Group mean and SD of R_1, PD, MTsat, and R_2^* parameter values in whole-brain GM and WM ROIs

	3T				7T			
	GM		WM		GM		WM	
	SC-EPI	FLASH	SC-EPI	FLASH	SC-EPI	FLASH	SC-EPI	FLASH
R_1 [s^{-1}]	0.72 ± 0.02	0.69 ± 0.01	1.13 ± 0.05	1.11 ± 0.04	0.52 ± 0.02	0.48 ± 0.02	0.73 ± 0.01	0.68 ± 0.01
PD [%]	78.5 ± 0.5	77.5 ± 0.4	68.9 ± 0.2	69.3 ± 0.2	81.0 ± 1.0	78.5 ± 0.6	69.1 ± 0.1	69.2 ± 0.1
MTsat [%][a]	1.82 ± 0.04	1.69 ± 0.04	3.6 ± 0.1	3.4 ± 0.1	0.7 ± 0.1	0.5 ± 0.1	1.7 ± 0.2	1.1 ± 0.1
R_2^* [s^{-1}]	17.9 ± 0.6	17.2 ± 0.5	20.1 ± 0.8	22.3 ± 0.7	37.3 ± 1.7	33.6 ± 1.4	36.8 ± 2.3	40.9 ± 2.0

[a] MTsat values at 7T are expected to vary across subjects and sequences due to different MTsat FAs applied.

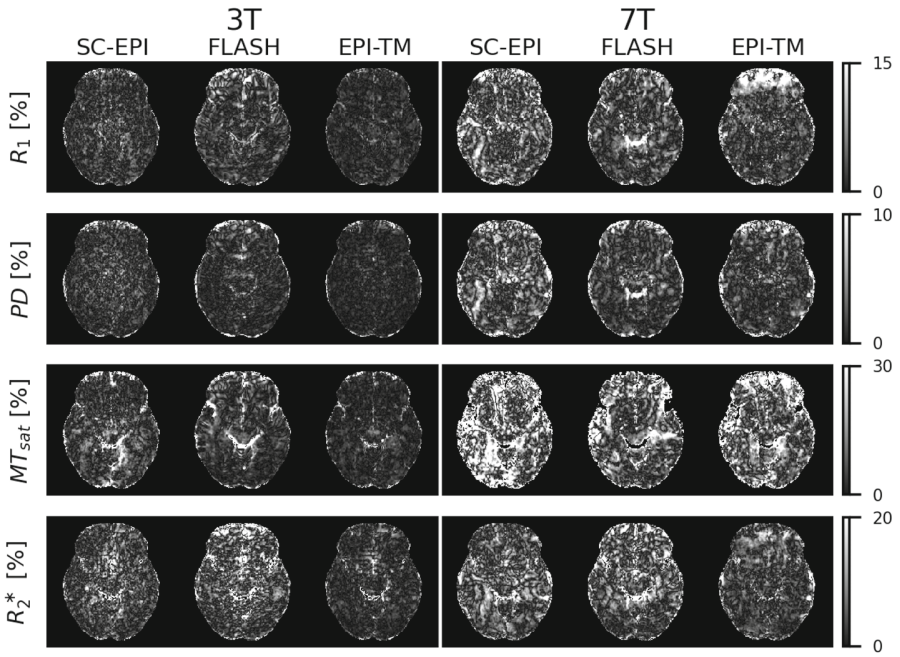

FIGURE 6 CoV of parameter maps shown for the representative subject in MNI space. The CoV was calculated across scan–rescan measurements

measures for FLASH in hippocampus (Figure 7, outlier). The time-matched EPI-TM (Figure 7, green) can achieve smaller RMS-CoV for all parameters except MTsat in CC. At 7T, RMS-CoV of PD was about twice as large compared to 3T. The CoV median of R_1 remained between 2% and 5% except for SC-EPI in pallidum. Such as at 3T, the CoVs for R_2^* were similar and below 15% for both sequences excluding outliers. MTsat showed higher CoVs across all ROIs for both sequences than at 3T, but SC-EPI in particular resulted in high CoV data points exceeding a tolerable range 0%–10%. Table 3 summarizes the mean and SD of the scan–rescan RMS-CoV of five subjects in whole-brain GM and WM regions, excluding outliers. WM and GM MTsat values at 7T as well as GM MTsat values at 3T had extremely large CoV values, which are considered unreliable. For completeness, the WM and GM RMS-CoV values for all parameters and all five subjects are listed in Supporting Information Table S1 with outliers marked.

4 | DISCUSSION

We presented a fast MPM protocol using skipped-CAIPI 3D-EPI at 3T and 7T and compared it with conventional FLASH-MPM. The SC-EPI protocol was designed to acquire all three contrasts at multiple TEs at 1 mm isotropic resolution in under 3 min, with good soft tissue contrasts. To answer whether the protocols could be translated into clinical research or cohort studies, we have conducted a scan–rescan reproducibility analysis. First, the absolute parameter values are discussed.

4.1 | Comparison of parameter maps

The multi-subject parameter comparison showed larger R_1 estimates of SC-EPI compared to FLASH. They may partly result from the small FA approximation and long TR approximation inherent to the MPM formalism.[35]

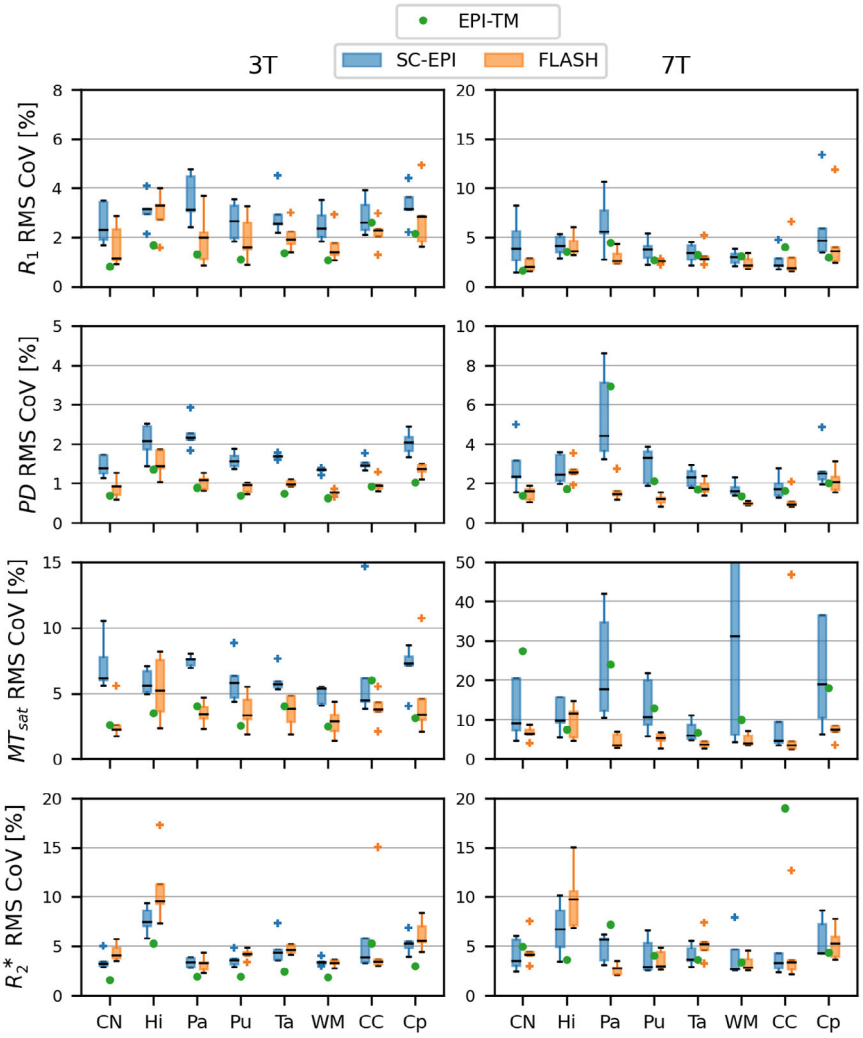

FIGURE 7 Distribution of R_1, PD, MTsat, and R_2^* RMS-CoV in ROIs across subjects at 3T and 7T (box plot). EPI-TM reflects the scan–rescan RMS-CoV of the single-subject SC-EPI scan time-matched to the FLASH scan. CN, caudate; Hi, hippocampus; Pa, pallidum; Pu, putamen; Ta, thalamus; WM: cerebral white matter; CC, body of corpus callosum; Cp, cerebellar peduncle. Outliers are marked as '+' in corresponding color.

TABLE 3 Group mean and SD of the scan–rescan RMS-CoV in whole-brain GM and WM ROIs

	3T				7T			
	GM		WM		GM		WM	
	SC-EPI	FLASH	SC-EPI	FLASH	SC-EPI	FLASH	SC-EPI	FLASH
R_1 [%]	3.4 ± 0.8	3.7 ± 0.4	2.8 ± 0.6	2.2 ± 0.6	6.5 ± 1.0	5.8 ± 0.3	4.0 ± 1.0	2.6 ± 0.4
PD [%]	2.1 ± 0.1	1.5 ± 0.2	1.6 ± 0.0	1.0 ± 0.1	3.8 ± 0.4	3.7 ± 1.5	2.3 ± 0.5	1.5 ± 0.2
MTsat [%]	$(8.8 \pm 0.6) \cdot 10^1$	$(2.0 \pm 1.1) \cdot 10^1$	5.8 ± 0.8	3.6 ± 1.3	$(1.1 \pm 0.6) \cdot 10^4$	$(1.6 \pm 1.0) \cdot 10^3$	$(2.6 \pm 3.6) \cdot 10^2$	$(2.2 \pm 2.0) \cdot 10^1$
R_2^* [%]	$(1.1 \pm 0.1) \cdot 10^1$	$(8.8 \pm 2.1) \cdot 10^1$	4.2 ± 0.5	7.7 ± 2.9	6.2 ± 1.5	$(1.0 \pm 0.4) \cdot 10^1$	3.7 ± 1.0	5.3 ± 2.1

Note: Outliers as identified in Supporting Information Table S1 have been excluded.

In fact, the latest version of hMRI toolbox v0.2.5 has an option to disable small FA approximation. However, it was not yet considered in this study. By signal simulations, it can be shown that prolonged TRs lead to higher R_1 MPM estimates closer to the ground truth, as demonstrated in Supporting Information Figure S4. Compared to FLASH, SC-EPI facilitates longer TRs in short TA without loss of scanning efficiency.[27] Thus, the R_1 estimates based on SC-EPI can be considered less biased by these MPM approximations. However, with the FAs and FLASH timing parameters used in this work, the MPM underestimation of R_1 should only amount to approximately 2%–3%. Although particularly narrow-banded excitation pulses have been used in this work, the side-bands were not zero; therefore, different TRs could still introduce different MT-biases of the R_1 estimation, whereby longer TRs

would be favorable (see below). In addition, a systematic difference in the estimation of R_2^* may contribute to the observed R_1 differences.

The observed R_2^* differences could be associated with different TE ranges in SC-EPI and FLASH. With multi-echo data analysis, signal extrapolated to TE = 0 is used for parameter estimation in the subsequent process of the hMRI toolbox.[9,38] This is done on the basis of R_2^*, which is estimated from the logarithm of the signal intensities at all TEs from all contrasts using a mono-exponential model (ESTATICS).[9,41] A mono-exponential R_2^* calculation based on data, that in fact involves multiple T_2^* compartments,[44,45] results in a linear combination of short and long T_2^* components.[46] The short T_2^* components may be attributed to bound water and the long component to free water.[45,47] The TE range of SC-EPI is better suited for estimation of long T_2^* components, whereas the TE range of FLASH is better suited for estimation of short T_2^* components. The mono-exponential T_2^* GM and WM estimates in this work ranged between about 20 and 60 ms, which may better be reflected by the TE range of SC-EPI. Hence, R_2^* and amplitude extrapolation at TE = 0 based on the FLASH data may be considered biased by comparably short T_2^* compartments and less sensitive to the prevalent, long T_2^* compartment. Furthermore, ESTATICS assumes that R_2^* remains constant across different contrasts. However, this assumption may be violated to varying degrees, depending on TR, as different compartments have different contributions to the signal in different contrasts, e.g., T_1 or MT weighting.[41]

Proton density values were calibrated to 69% in WM.[38] Consequently, no difference between SC-EPI and FLASH is observed in WM, apart from a minor variance that can be explained by differences in the WM masks used for the hMRI calibration and our evaluation. The difference of R_1 estimation in GM was translated to PD, resulting in 1.3% and 2.5% PD difference in GM at 3T and 7T, respectively. The HC-BC receive field correction at 3T is expected to introduce residual body coil sensitivity inhomogeneities to PD maps.[10,36] Supporting Information Figure S5 shows only small differences between the PD maps corrected using the HC-BC method and Unified Segmentation on representative 3T data.

MTsat is a semi-quantitative parameter. At 3T, with the same MT pulse, MTsat increases slightly with longer TR of SC-EPI.[48] However, at 7T, due to SAR limitations, SC-EPI, and FLASH had different MT FAs across subjects, and longer TR of SC-EPI allowed for a larger MT FA than FLASH, which also lead to considerably larger MTsat. Overall, MTw acquisitions at 7T suffered significantly from B_1^+ inhomogeneity and SAR limitations, regardless of the sequence used. In particular, in the temporal lobes and the cerebellum, the actual MT pulse FAs were so small, that MTsat in these regions were not interpretable.

4.2 | Transmit correction due to B_0 inhomogeneities

The long water excitation pulse that we applied in this study required a novel, adapted transmit correction approach. By using such a long rectangular pulse compared to typical short rectangular pulses (~0.1 ms), a significant T_1 bias by MT saturation can be avoided.[23,49] Even though the rectangular pulse has an uneven frequency response, it provides the benefit of an analytical expression for the effective FA as a function of off-resonance. We used this to derive an analytical B_0 correction of the transmit correction factor. Homogeneity of quantitative PD, R_1, and MTsat depend on this correction factor. In this study, additional B_0 field maps were used to compensate for the reduced off-resonance FA when using long RF pulse.[34] The influence of the B_0 correction is mainly located in prefrontal brain regions. In these areas, the deviation from the conventional correction factor without B_0 consideration was about 5%.

Although narrow-banded RF pulses (2.4 ms [3T]/1.0 ms [7T]) may not be necessary for fat suppression with FLASH, RF pulses longer than 0.1 ms should be strongly considered given the MT bias on apparent R_1 and MTsat estimates. In this case, the proposed B_0 correction of the transmit field correction factor should be considered also for FLASH. Alternatively, the T_1 bias can be tackled by numerically optimized pulses that have a flat frequency response.[23] In addition, the bandwidth could be tailored to suppress fat, however, at the cost of even longer pulses than the rectangular pulses that we used.

4.3 | Analysis of inter-scan CoV

The main purpose of this work was to investigate reproducibility. Our proposed SC-EPI-MPM acquisition protocol achieved good reproducibility compared with FLASH. At 3T, single measurement SC-EPI takes about one-fifth of the TA of FLASH. With roughly half of the SNR, the RMS-CoV of SC-EPI was 1.2–1.7 times larger than that of FLASH for all parameters. R_2^* of SC-EPI even achieved reduced CoV in both GM and WM (Figure 7). The calibration of PD estimates of WM to 69% might lead to an underestimation of CoV in WM and mitigate that in GM. The observed CoV in deep brain GM regions, WM structures and whole-brain GM and WM was up to two times lower than the intra-site RMS-CoV in a recent multicenter dual-vendor study, which ranged from 2% to 10% for

R_1, 5% to 15% for MTsat, and 10% to 30% for R_2^* (outliers excluded).[10] The group-average intra-subject CoV of SC-EPI was also in the same order of magnitude as the average intra-subject CoV of a FLASH-MPM protocol optimized for the clinical routine acquired at 1.6 mm isotropic resolution within 7 min.[11] By averaging two SC-EPI scans, or by reducing parallel imaging by a factor of two, a similar TA could be approached at 1 mm isotropic resolution, while improving reproducibility. Thus, we conclude that the presented SC-EPI-MPM protocol at 3T has the potential to be implemented in a multicenter study and clinical research.

The reproducibility of MPM at 7T was reported in a previous study at 0.5 mm isotropic resolution without MTw acquisition obtained within 20 min.[50] The scan–rescan CoV ranged from 4.2% to ~8% for PD, from 6.5% to 16% for R_1, from 10% to 20% for R_2^* (outliers excluded). A scan–rescan CoV improvement of more than 10% was reported when engaging prospective motion correction and dynamic B_0 correction. In our study, the FLASH protocol was modified based on the vendor FLASH sequence toward sequence parameters similar to the SC-EPI sequence at 7T. The RMS-CoV of the 1 mm 7T FLASH protocol acquired in 4.5 min achieved good values across ROIs comparable to,[50] although the overall level was increased compared to that of the 3T FLASH. SC-EPI at 7T, acquired in 2 min, showed a similar pattern of CoVs across ROIs as at 3T, indicating a good reproducibility at high field strength, except for MTsat. The RMS-CoV of SC-EPI was ~1.2 times larger than that of FLASH for R_1, while it was ~0.8 times smaller than FLASH for R_2^*. Together with the reduced RMS-CoV of R_2^* at 3T, this is a strong indication that the extended range of TEs (and longer TRs) is beneficial in terms of R_2^* reproducibility.

As indicated before, MT pulse homogeneity at 7T remains a problem in our study, even with the help of dielectric bags. Different reference voltage and MT FA further lead to variability of CoV in MTsat. Overall, this makes a serious interpretation of RMS-CoV values for MTsat at 7T impossible.

Furthermore, the RF receive field correction for PD map estimation at 7T was degraded by the limitations of numerical post-processing methods and unreliable MTsat estimation. Numerical estimation of the receive field bias requires the WM and GM probability maps, which are derived from the segmentation of the calculated MTsat map within the hMRI toolbox.[37] Therefore, the poor and nonuniform soft tissue contrasts in MTsat maps and different MT saturation effect in different subjects may have resulted in increased intra-scan CoV of PD and variability across subjects at 7T for both FLASH and SC-EPI.

The inter-scan variability of R_1 of all ROIs, on the other hand, was very comparable, except for some data points in pallidum (Figure 7). The slightly elevated CoV of SC-EPI for R_1 mainly came from reduced SNR. The time-match SC-EPI single-subject data at 7T indicated higher reproducibility, aligning with FLASH in both deep brain GM regions, cerebral WM structures as well as whole-brain GM and WM (Table 3). At 3T, even lower RMS-CoV values than with FLASH seem possible, if more time is invested in data acquisition by reducing parallel imaging or averaging.

Unlike previous studies,[9–11] both R_2^* and MTsat showed better reproducibility in our study. At 3T, RMS-CoV for R_2^* was smaller than what was reported before[10] across most of the ROIs excluding some data points (of the same subject) in the corpus callosum. Even in the hippocampus, where both single-measurement SC-EPI and FLASH shared the highest RMS-CoV for R_2^*, they are still lower than the intra-site CoV (24%–32%, outliers excluded) in a previous study.[10] The time-matched SC-EPI reached the smallest RMS-CoV for R_2^* in most of the ROIs, e.g., 5.3% in the hippocampus. Similar tendency was found in 7T data sets with slightly increased overall CoV and variability across subjects.

MTsat is sensitive to changes in MT pulse, field inhomogeneities or R_1 values. In particular, it depends on the power and offset frequency of the MT pulse.[48] FLASH showed relatively small RMS-CoV of MTsat at both 3T and 7T. SC-EPI had a decent performance at 3T, which is comparable to the previous study,[10] but showed much higher variability at 7T. The RMS-CoV of MTsat in whole-brain WM and GM also indicated strong inhomogeneities, among which only RMS-CoV values in WM at 3T were found to be meaningful. Further studies on the reduction of MT pulse inhomogeneity at ultra-high fields need to be conducted, for example using Direct Saturation Control (DSatC),[51] which showed significant improvements at 7T.

4.4 | Limitations and future prospects

To keep differences to the gold standard protocol small, we did not optimize FAs for prolonged TRs, which could be investigated in the future. Interestingly, preliminary Monte-Carlo simulations for a range of typical T_1 values in the brain (Supporting Information Figure S4) suggest that increasing FAs at longer TRs would barely alter precision (and therefore reproducibility), whereas longer TRs (20–60 ms) at fixed FAs of 4° and 25°, would increase precision and reduce bias at the same time compared to the gold standard. Motion correction was not considered in this study. Prospective motion correction has recently been used for higher resolution MPM with great success.[50,53] Furthermore, a weighted-averaging method has recently been proposed to improve the stability of parameter maps in regions, where artifacts induced by subject motion are

assumed to show as increased R_2^* fit errors.[54] This requires at least two scans, which leads to even longer FLASH measurements. Multiple fast SC-EPI scans in reasonable scan time could benefit particularly well from this approach compared to the plain raw data averaging performed in this work for the time-matched comparison. This may also help to mitigate the effect of physiological noise on MPM. In fact, Figure 4 shows some apparent left–right R_1 asymmetry using SC-EPI and EPI-TM at 7T, which may be attributed to respiration-induced local signal variation that can be observed in the corresponding raw data. In this example, plain averaging with the second scan (EPI-TM) did not entirely counterbalance the artifact of the first scan. The weighted-averaging approach may minimize this bias better. Gradient echo sequences at late TEs and ultra-high fields are particularly affected by physiologically induced field perturbations, and accounting for field perturbations during image reconstruction improves image quality and derived maps.[50,55,56] Similar approaches could be applied to SC-EPI as well. At ultra-high fields, physiological noise becomes dominant over thermal noise at comparably large voxel sizes of 1 mm^3 such that smaller voxel sizes for SC-EPI may be preferable.[57,58] In a current 7T project, we optimize joint SC-EPI-based MPM and quantitative susceptibility mapping at 0.6 mm isotropic resolution using parallel transmission,[59] aiming to identify new imaging biomarkers that can detect early disease manifestations.

5 | CONCLUSIONS

We presented a novel, whole-head MPM acquisition at 1 mm isotropic resolution in less than 3 min using a fast multi-contrast, multi-echo skipped-CAIPI 3D-EPI sequence at 3T and 7T. Owing to high segmentation factors and optimized parallel imaging, the SC-EPI-MPM protocol at 3T (~3 min) provides precise quantitative maps of PD, R_1, R_2^*, and MTsat, even in deep brain regions, with high reproducibility and without severe artifacts or distortions, when compared with literature values obtained in much longer scan time or using larger voxel sizes. At 7T, within 2 min decent parameter maps can be obtained; however, reproducibility is degraded, not least due to ultra-high field-specific challenges yet to be solved. Considering the short TA, high resolution and good reproducibility, we conclude that a SC-EPI-based MPM protocol can be translated into clinical research or longitudinal studies.

ACKNOWLEDGMENTS

This work received financial support from the European Union Horizon 2020 Research and Innovation program under grant agreement 885876 (AROMA) and through the German Federal Ministry of Education and Research (Bundesministerium für Bildung und Forschung; funding code 01ED2109A) as part of the SCAIFIELD project under the aegis of the EU Joint Programme—Neurodegenerative Disease Research (JPND) (www.jpnd.eu). Open access funding enabled and organized by Projekt DEAL.

DATA AVAILABILITY STATEMENT

An automated script of the entire analysis pipeline and example data are made available at https://github.com/mrphysics-bonn/MPM. The authors are open to share SC-EPI pulse sequence binaries upon request via C2P procedure (Siemens Healthineers).

ORCID

Difei Wang https://orcid.org/0000-0002-7983-2648
Philipp Ehses https://orcid.org/0000-0002-5839-6525
Tony Stöcker https://orcid.org/0000-0002-8946-9141
Rüdiger Stirnberg https://orcid.org/0000-0001-7021-1063

REFERENCES

1. Bender AR, Keresztes A, Bodammer NC, et al. Optimization and validation of automated hippocampal subfield segmentation across the lifespan. *Hum Brain Mapp*. 2018;39:916-931.
2. Xie L, Wisse LEM, Pluta J, et al. Automated segmentation of medial temporal lobe subregions on in vivo T1-weighted MRI in early stages of Alzheimer's disease. *Hum Brain Mapp*. 2019;40:3431-3451.
3. Du G, Lewis MM, Sica C, Kong L, Huang X. Magnetic resonance T1w/T2w ratio: a parsimonious marker for Parkinson disease. *Ann Neurol*. 2019;85:96-104.
4. Meijer FJA. Brain MRI in Parkinson's disease. *Front Biosci*. 2014;E6:360 10.2741/E711, 6, 369.
5. Winter JD, Estrada M, Cheng H-LM. Normal tissue quantitative T1 and T2* MRI relaxation time responses to hypercapnic and hyperoxic gases. *Acad Radiol*. 2011;18:1159-1167.
6. Warach S, Gaa J, Siewert B, Wielopolski P, Edelman RR. Acute human stroke studied by whole brain echo planar diffusion-weighted magnetic resonance imaging. *Ann Neurol*. 1995;37:231-241.
7. Gandon Y, Olivié D, Guyader D, et al. Non-invasive assessment of hepatic iron stores by MRI. *Lancet*. 2004;363:357-362.
8. Bakshi R, Ariyaratana S, Benedict RHB, Jacobs L. Fluid-attenuated inversion recovery magnetic resonance imaging detects cortical and Juxtacortical multiple sclerosis lesions. *Arch Neurol*. 2001;58:742-748.
9. Weiskopf N, Suckling J, Williams G, et al. Quantitative multi-parameter mapping of R1, PD*, MT, and R2* at 3T: a multi-center validation. *Front Neurosci*. 2013;7:1-11.
10. Leutritz T, Seif M, Helms G, et al. Multiparameter mapping of relaxation (R1, R2*), proton density and magnetization transfer saturation at 3 T: a multicenter dual-vendor reproducibility and repeatability study. *Hum Brain Mapp*. 2020;41:4232-4247.
11. Cooper G, Hirsch S, Scheel M, et al. Quantitative multi-parameter mapping optimized for the clinical routine. *Front Neurosci*. 2020;14:1-9.

12. Breuer FA, Blaimer M, Mueller MF, et al. Controlled aliasing in volumetric parallel imaging (2D CAIPIRINHA). *Magn Reson Med*. 2006;55:549-556.
13. Stirnberg R, Stöcker T. Segmented K-space blipped-controlled aliasing in parallel imaging for high spatiotemporal resolution EPI. *Magn Reson Med*. 2021;85:1540-1551.
14. Feinberg DA, Oshio K. Phase errors in multi-shot echo planar imaging. *Magn Reson Med*. 1994;32:535-539.
15. Sati P, Thomasson D, Li N, et al. Rapid, high-resolution, whole-brain, susceptibility-based MRI of multiple sclerosis. *Mult Scler J*. 2014;20:1464-1470.
16. Zwanenburg JJM, Versluis MJ, Luijten PR, Petridou N. Fast high resolution whole brain T2* weighted imaging using echo planar imaging at 7T. *Neuroimage*. 2011;56:1902-1907.
17. Norbeck O, Sprenger T, Avventi E, et al. Optimizing 3D EPI for rapid T 1 -weighted imaging. *Magn Reson Med*. 2020;84:1441-1455.
18. Stirnberg R, Deistung A, Reichenbach J, Stöcker T. Accelerated quantitative susceptibility and R2* mapping with flexible k-t-segmented 3D-EPI. In: *Proceedings of the Joint Annual Meeting of ISMRM-ESMRMB*, Paris, France. 2018;2: 50–53.
19. Baglieri A, Marino MA, Morabito R, Lorenzo G, Bramanti P, Marino S. Differences between conventional and nonconventional MRI techniques in Parkinson's disease. *Funct Neurol*. 2013;28:73-82.
20. Webb AG. Dielectric materials in magnetic resonance. *Concepts Magn Reson Part A*. 2011;38A:148-184.
21. Jellus V, Kannengiesser ARS. Adaptive coil combination using a body coil scan as phase reference. In: *Proceedings of the Joint Annual Meeting of ISMRM-ESMRMB*, Milan, Italy. 2014;22:4406.
22. Stirnberg R, Brenner D, Stöcker T, Shah NJ. Rapid fat suppression for three-dimensional echo planar imaging with minimized specific absorption rate. *Magn Reson Med*. 2016;76:1517-1523.
23. Olsson H, Andersen M, Lätt J, Wirestam R, Helms G. Reducing bias in dual flip angle T1 -mapping in human brain at 7T. *Magn Reson Med*. 2020;84:1347-1358.
24. Callaghan MF, Lutti A, Ashburner J, et al. Example dataset for the hMRI toolbox. *Data Brief*. 2019;25:104132.
25. Callaghan MF, Lutti A, Ashburner J, et al. MPM_protocol_vendor_seq_SIEMENS_settings.pdf. Accessed September 9, 2019. https://hmri-group.github.io/hMRI-toolbox/#hmri-example-data-and-mri-protocol.
26. Ivanov D, Barth M, Uludag K, Poser BA. Robust ACS acquisition for 3D echo planar imaging. In: *Proceedings of the 23rd Annual Meeting of ISMRM*, Toronto, Ontario, Canada. 2015; 2059.
27. Deichmann R, Adolf H, Nöth U, Kuchenbrod E, Schwarzbauer C, Haase A. Calculation of signal intensities in hybrid sequences for fast NMR imaging. *Magn Reson Med*. 1995;34:481-489.
28. Hendriks AD, D'Agata F, Raimondo L, et al. Pushing functional MRI spatial and temporal resolution further: high-density receive arrays combined with shot-selective 2D CAIPIRINHA for 3D echo-planar imaging at 7 T. *NMR Biomed*. 2020; 33:1-13.
29. Brenner D, Stirnberg R, Pracht ED, Stöcker T. Two-dimensional accelerated MP-RAGE imaging with flexible linear reordering. *Magn Reson Mater Phys Biol Med*. 2014;27:455-462.
30. van der Kouwe AJW, Benner T, Salat DH, Fischl B. Brain morphometry with multiecho MPRAGE. *Neuroimage*. 2008;40:559-569.
31. Ehses P, Brenner D, Stirnberg R, Pracht ED, Stöcker T. Whole-brain B1-mapping using three-dimensional DREAM. *Magn Reson Med*. 2019;82:924-934.
32. Nehrke K, Börnert P. DREAM – a novel approach for robust, ultrafast, multislice B 1 mapping. *Magn Reson Med*. 2012;68:1517-1526.
33. Nehrke K, Versluis MJ, Webb A, Börnert P. Volumetric B_1 (+) mapping of the brain at 7T using DREAM. *Magn Reson Med*. 2014;71:246-256.
34. Freed DE, Hürlimann MD, Scheven UM. The equivalence between off-resonance and on-resonance pulse sequences and its application to steady-state free precession with diffusion in inhomogeneous fields. *J Magn Reson*. 2003;162:328-335.
35. Helms G, Dathe H, Dechent P. Quantitative FLASH MRI at 3T using a rational approximation of the Ernst equation. *Magn Reson Med*. 2008;59:667-672.
36. Volz S, Nöth U, Deichmann R. Correction of systematic errors in quantitative proton density mapping. *Magn Reson Med*. 2012;68:74-85.
37. Ashburner J, Friston KJ. Unified segmentation. *Neuroimage*. 2005;26:839-851.
38. Tabelow K, Balteau E, Ashburner J, et al. hMRI – a toolbox for quantitative MRI in neuroscience and clinical research. *Neuroimage*. 2019;194:191-210.
39. Preibisch C, Deichmann R. Influence of RF spoiling on the stability and accuracy of T1 mapping based on spoiled FLASH with varying flip angles. *Magn Reson Med*. 2009; 61:125-135.
40. Malik SJ, Teixeira RPAG, Hajnal JV. Extended phase graph formalism for systems with magnetization transfer and exchange. *Magn Reson Med*. 2018;80:767-779.
41. Weiskopf N, Callaghan MF, Josephs O, Lutti A, Mohammadi S. Estimating the apparent transverse relaxation time (R2*) from images with different contrasts (ESTATICS) reduces motion artifacts. *Front Neurosci*. 2014;8:1-10.
42. Tofts P. *Quantitative MRI of the Brain: Measuring Changes Caused by Disease*. John Wiley & Sons; 2003.
43. Ashburner J. A fast diffeomorphic image registration algorithm. *Neuroimage*. 2007;38:95-113.
44. Lancaster JL, Andrews T, Hardies LJ, Dodd S, Fox PT. Three-pool model of white matter. *J Magn Reson Imaging*. 2003;17:1-10.
45. Hwang D, Kim D-H, Du YP. In vivo multi-slice mapping of myelin water content using T2* decay. *Neuroimage*. 2010;52:198-204.
46. Juras V, Apprich S, Szomolanyi P, Bieri O, Deligianni X, Trattnig S. Bi-exponential T2*analysis of healthy and diseased Achilles tendons: an in vivo preliminary magnetic resonance study and correlation with clinical score. *Eur Radiol*. 2013;23:2814-2822.
47. Du J, Diaz E, Carl M, Bae W, Chung CB, Bydder GM. Ultrashort echo time imaging with bicomponent analysis. *Magn Reson Med*. 2012;67:645-649.
48. Helms G, Dathe H, Kallenberg K, Dechent P. High-resolution maps of magnetization transfer with inherent correction for RF inhomogeneity and T1 relaxation obtained from 3D FLASH MRI. *Magn Reson Med*. 2008;60:1396-1407.

49. Teixeira RP AG, Neji R, Wood TC, Baburamani AA, Malik SJ, Hajnal JV. Controlled saturation magnetization transfer for reproducible multivendor variable flip angle T1 and T2 mapping. *Magn Reson Med*. 2020;84:221-236.
50. Vaculčiaková L, Podranski K, Edwards LJ, et al. Combining navigator and optical prospective motion correction for high-quality 500 µm resolution quantitative multi-parameter mapping at 7T. *Magn Reson Med*. 2022;88:787-801.
51. Leitão D, Tomi-tricot R, Liebig P, et al. Direct saturation control for magnetization transfer imaging at 7T. In: *Proceedings of the ISMRM & SMRT Virtual Conference & Exhibition*, Sydney, Australia. 2020;Abstract 0607.
52. Callaghan MF, Josephs O, Herbst M, Zaitsev M, Todd N, Weiskopf N. An evaluation of prospective motion correction (PMC) for high resolution quantitative MRI. *Front Neurosci*. 2015;9:1-9.
53. Streubel T, Klock L, Callaghan S, et al. Identification and correction of errors in quantitative multi-parameter mapping. In: *Proceedings of the ISMRM & SMRT Virtual Conference & Exhibition*, Sydney, Australia. 2020;Abstract 1016.
54. Van de Moortele P-F, Pfeuffer J, Glover GH, Ugurbil K, Hu X. Respiration-induced B0 fluctuations and their spatial distribution in the human brain at 7 tesla. *Magn Reson Med*. 2002;47:888-895.
55. Versluis MJ, Peeters JM, Rooden S, et al. Origin and reduction of motion and f0 artifacts in high resolution T2*-weighted magnetic resonance imaging: application in Alzheimer's disease patients. *Neuroimage*. 2010;51:1082-1088.
56. Zwaag W v d, Marques JP, Kober T, Glover G, Gruetter R, Krueger G. Temporal SNR characteristics in segmented 3D-EPI at 7T. *Magn Reson Med*. 2012;67:344-352.
57. Triantafyllou C, Hoge RD, Krueger G, et al. Comparison of physiological noise at 1.5 T, 3 T and 7 T and optimization of fMRI acquisition parameters. *Neuroimage*. 2005;26:243-250.
58. Le Ster C, Moreno A, Mauconduit F, et al. Comparison of SMS-EPI and 3D-EPI at 7T in an fMRI localizer study with matched spatiotemporal resolution and homogenized excitation profiles. *PLOS One*. 2019;14:e0225286.

SUPPORTING INFORMATION

Additional supporting information may be found in the online version of the article at the publisher's website.

TABLE S1 The scan–rescan RMS-CoV of all four parameters in whole-brain GM and WM ROIs for all five subjects. Outliers (enclosed in brackets), which exceed the first and third quartile by more than 1.5 times the interquartile range, are excluded from the mean and standard deviation reported in Table 3. Extremely large MTsat RMS-CoV values in WM and GM at 7 T and in GM at 3 T are considered unreliable.

FIGURE S1: Axial and sagittal slices of the FLASH MTw images acquired with 0.4 ms short RF pulse (top) and 2.45 ms long RF pulse for water excitation (bottom). The default non-selective RF pulse duration is 0.4 ms. The shortest (left) and the longest (right) TE images are shown. In this TE range, signal dropouts above the sinus are dominated by the narrow-banded RF pulse. Up to a certain level, signal bias quantification can be counterbalanced by the proposed B_0 correction. However, quantification results will be inappropriate for too low SNR.

FIGURE S2: Parameter maps of SC-EPI, FLASH and EPI-TM for a single subject scanned at 3 and 7 T (same data as shown in Figure 4) viewed in sagittal orientation. The MTsat map of FLASH at 7 T was multiplied by a factor of 1.4. The f_T (transmit field correction) maps are shown along with difference to the conventional correction map without B_0 correction, as well as the corresponding off-resonance map, $\Delta\omega$. It shows that susceptibility artifacts are mainly located around the sinus. In particular, the R_2^* maps using SC-EPI and EPI-TM show clearer susceptibility-related bias in these regions, which may be attributed to images with much longer TEs involved in the fit (the raw weighted SC-EPI images at the shortest TE do not show more susceptibility-induced artifacts than the corresponding FLASH images, cf. Figure 3).

FIGURE S3: Phantom R_1 and R_2^* results at 3 T. A homogeneous, single compartment phantom (top left) filled with 75.35% distilled water, 23% polyvinylpyrrolidone K30, 1% agarose, and 0.65% NaCl was used. Measured by inversion recovery and spin-echo spectroscopic sequences, bulk ground truth relaxation times were estimated as $T_1 = 1.475 \pm 0.015$ s ($R_1 = 0.678 \pm 0.007$ s^{-1}, the black dashed line), $T_2 = 66.6 \pm 0.18$ ms. Accordingly, $T_2^* < 66.6$ ms, and therefore $R_2^* > 15.01$ s^{-1} is expected. The bar plot (right) shows the R_1 and R_2^* estimates acquired with the MPM protocols of SC-EPI (blue), FLASH (orange) and FLASH with TR and TEs matched to SC-EPI (FLASH-long TR, green). Three circular ROIs, each containing 8697 voxels, were chosen. The red line indicates the position and diameter of each ROI (bottom left). The results are consistent with the in-vivo results: R_1 estimates of SC-EPI were ∼3.4% higher than R_1 estimates of FLASH. The R_1 estimates acquired with SC-EPI are closer to the ground truth R_1 value of the phantom. R_2^* estimates of SC-EPI were ∼8.0% higher than R_2^* estimates of FLASH, which is consistent with the GM results obtained at 3 T. The FLASH-long TR results seem to better agree with SC-EPI results obtained with the same TRs and TEs, suggesting a sequence parameter bias.

FIGURE S4: Results of MPM Monte-Carlo simulations to estimate T_1. Noise-free signals were generated for each combination of TR and T_1w flip angle α_{T1} in the displayed range according to the ideal, perfectly-spoiled steady-state equation with unity equilibrium magnetization and a ground truth $T_1 = 1$, 2, and 4 ms. The flip angle of PDw signal was fixed at a gold standard 4° (left) and 6 (right). 20 000 instances of Gaussian noise with a standard deviation of $\sqrt{2}/1000$ were added to both T_1w and PDw (corresponds to an SNR of 20–65 in the PDw image, depending

on flip angles, TR and ground truth T_1). From the corresponding signal magnitudes T_1 was estimated using Equation 9a in.[35] The standard deviation refers to the precision of the T_1 estimations. The percentage error refers to the bias of the T_1 estimation to the ground truth T_1. The 0.0-contour line in the percentage error plot indicates the most accurate T_1 estimation. Increasing flip angles at longer TRs than the gold standard TR would alter precision, and therefore reproducibility, only little (e.g., at TR = 40 ms, move upward from FA = 25°). However, longer TRs (30–60 ms) at fixed gold standard flip angles of 4° and 25°, would increase precision and reduce bias at the same time for a range of typical T_1 values in the brain (e.g., at FA = 25°, move to the right from TR = 20 ms).

FIGURE S5: PD maps in percentage units of SC-EPI, EPI-TM and FLASH for a single subject at 3 T. The RF receive field correction is done once by head coil-body coil (HC-BC) method and Unified Segmentation (US). The ratio of HC-BC over US indicates slight differences between two methods in the order of ±5%.

How to cite this article: Wang D, Ehses P, Stöcker T, Stirnberg R. Reproducibility of rapid multi-parameter mapping at 3T and 7T with highly segmented and accelerated 3D-EPI. *Magn Reson Med*. 2022;88:2217-2232. doi: 10.1002/mrm.29383

WOULD YOU LIKE TO POST AN INFORMAL COMMENT ABOUT THIS PAPER, OR ASK THE AUTHORS A QUESTION ABOUT IT?

If so, please visit https://mrm.ismrm.org/ and register for our Magn Reson Med Discourse site (registration is free).

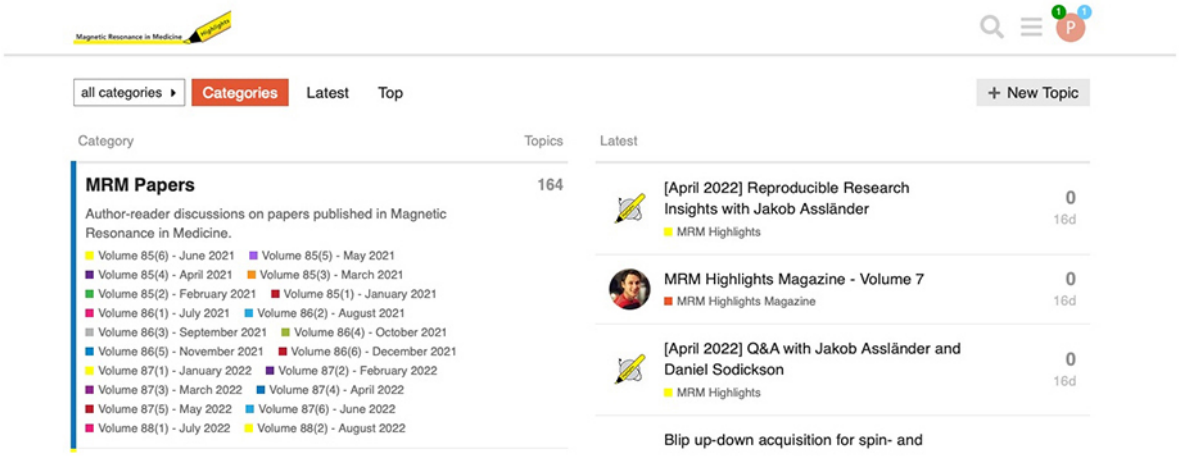

Magn Reson Med is currently listing the top 8 downloaded papers from each issue (including Editor's Picks) for comments and questions on the Discourse web site.

However, we are happy to list this or any other papers (please email mrm@ismrm.org to request the posting of any other papers.)

We encourage informal comment and discussion about Magn Reson Med papers on this site. Please note, however, that a formal errata from the authors should still be submitted in the usual way via our Manuscript Central online submission system.